Journal of Biomechanics ∎ (∎∎∎∎) ∎∎∎–∎∎∎

Contents lists available at ScienceDirect

Journal of Biomechanics

journal homepage: www.elsevier.com/locate/jbiomech
www.JBiomech.com

Spatial variations in Achilles tendon shear wave speed

Ryan J. DeWall [a,b,*], Laura C. Slane [c], Kenneth S. Lee [a], Darryl G. Thelen [c,d]

[a] Department of Radiology, University of Wisconsin-Madison, Madison, WI, USA
[b] Department of Medical Physics, University of Wisconsin-Madison, Madison, WI, USA
[c] Department of Biomedical Engineering, University of Wisconsin-Madison, Madison, WI, USA
[d] Department of Mechanical Engineering, University of Wisconsin-Madison, Madison, WI, USA

ARTICLE INFO

Article history:
Accepted 12 May 2014

Keywords:
Noninvasive mechanics
Shear wave imaging
Shear wave elastography
Tendon mechanics
Ultrasound elastography

ABSTRACT

Supersonic shear imaging (SSI) is an ultrasound imaging modality that can provide insight into tissue mechanics by measuring shear wave propagation speed, a property that depends on tissue elasticity. SSI has previously been used to characterize the increase in Achilles tendon shear wave speed that occurs with loading, an effect attributable to the strain-stiffening behavior of the tissue. However, little is known about how shear wave speed varies spatially, which is important, given the anatomical variation that occurs between the calcaneus insertion and the gastrocnemius musculotendon junction. The purpose of this study was to investigate spatial variations in shear wave speed along medial and lateral paths of the Achilles tendon for three different ankle postures: resting ankle angle (R, i.e. neutral), plantarflexed (P; R − 15°), and dorsiflexed (D; R+15°). We observed significant spatial and posture variations in tendon shear wave speed in ten healthy young adults. Shear wave speeds in the Achilles free tendon averaged 12 ± 1.2 m/s in a resting position, but decreased to 7.2 ± 1.8 m/s with passive plantarflexion. Distal tendon shear wave speeds often reached the maximum tracking limit (16.3 m/s) of the system when the ankle was in the passively dorsiflexed posture (+15° from R). At a fixed posture, shear wave speeds decreased significantly from the free tendon to the gastrocnemius musculotendon junction, with slightly higher speeds measured on the medial side than on the lateral side. Shear wave speeds were only weakly correlated with the thickness and depth of the tendon, suggesting that the distal-to-proximal variations may reflect greater compliance in the aponeurosis relative to the free tendon. The results highlight the importance of considering both limb posture and transducer positioning when using SSI for biomechanical and clinical assessments of the Achilles tendon.

1. Introduction

Achilles tendon injury, e.g. tendinopathy, can lead to chronic pain and impairment. The choice of treatment depends, in part, on the location and extent of injury. For example, conservative treatments such as eccentric exercises are more successful in treating mid-substance tendinopathy than in treating insertional tendinopathy at the calcaneus (Fahlstrom et al., 2003). However, identifying the location and severity of injury can be challenging, in part due to the complexity of Achilles tendon anatomy and mechanics. The Achilles tendon arises as the shared aponeurosis of the soleus, lateral gastrocnemius, and medial gastrocnemius (Wickiewicz et al., 1983), with each muscle exhibiting unique architectural features (Ward et al., 2009). The medial gastrocnemius has a larger physiological cross-section and more distal muscle–tendon junction than the lateral gastrocnemius (Ward et al., 2009; Wickiewicz et al., 1983), while the soleus inserts onto the Achilles tendon from the posterior side. Anatomical studies suggest that there is substantial inherent variability in these regional architectural features (O'Brien, 1984), which may factor into the location and presentation of tendon injury in an individual. Hence, there is a need for an improved understanding of the relationship between tendon anatomy and spatial mechanics, which could improve our ability to distinguish normal regional variations in tendon mechanics from those arising from tendon injury.

Ultrasound is often used to noninvasively elucidate tendon mechanics. For example, cine ultrasonic imaging can be used to track Achilles tendon motion and stretch with loading (Maganaris, 2003; Maganaris and Paul, 1999, 2002; Peixinho et al., 2008). Prior studies have identified spatial differences in tendon deformation, noting differences in stretch in the aponeurosis and the tendon for the same external load (Arampatzis et al., 2005; Arndt et al., 1998; Finni et al., 2003; Kubo et al., 1999; Maganaris and Paul, 1999; Magnusson et al., 2001, 2003; Muramatsu et al., 2001).

* Corresponding author at: Department of Radiology 1111 Highland Ave Madison, WI 53705, USA. Tel.: +1 616 405-9172.
E-mail address: ryandewall@gmail.com (R.J. DeWall).

http://dx.doi.org/10.1016/j.jbiomech.2014.05.008
0021-9290/

Additionally, imaging techniques broadly referred to as elastography have been applied to tendon biomechanics. Strain imaging, one form of ultrasound elastography capable of measuring high-resolution axial strain (Ophir et al., 1991), has been used to study tendon injuries. Tendon strain has been shown to be elevated in tendinopathic patients relative to healthy control subjects (De Zordo et al., 2010, 2009).

Ultrasound shear wave imaging techniques have emerged for mapping shear wave speeds within tissue (Bercoff et al., 2004; Nightingale et al., 2002; Sandrin et al., 2003). A technique called Supersonic Shear Imaging (SSI) generates shear waves using focused acoustic beams (i.e. acoustic radiation force) and then uses ultra-high frame rate ultrasonic imaging (Bercoff et al., 2004) to track these waves as they propagate. Shear wave speed can then be used as a non-invasive metric of tissue stiffness (D'Onofrio et al., 2010), because of its relationship to the shear modulus (Bercoff et al., 2004). SSI has previously demonstrated its ability to detect localized pathological changes in the stiffness of a variety of soft tissues, such as the breast, liver, and thyroid (Athanasiou et al., 2010; Bavu et al., 2011; Sebag et al., 2010). More recently, this method has been used to characterize activation- and length-dependent stiffness changes in muscle (Bouillard et al., 2011; Chernak et al., 2013; Gennisson et al., 2010; Koo et al., 2013; Maisetti et al., 2012; Nordez and Hug, 2010).

The application of SSI to tendon, however, has been studied less extensively. Shear wave speed in the free Achilles tendon has been measured (Arda et al., 2011; Aubry et al., 2013; Brum et al., 2014; Chen et al., 2013; Hug et al., 2013) and has been shown to increase as the tendon is stretched (Aubry et al., 2011, 2013). In the ruptured Achilles tendon, shear wave speed was significantly lower than in healthy tendons, and subsequently increased during the healing phase (Chen et al., 2013). In an *ex vivo* porcine partial tear model, regional shear wave speed was altered in the vicinity of tear damage (DeWall et al., 2014). SSI has also shown the onset of the rise in tension of the Achilles tendon with passive dorsiflexion (Hug et al., 2013). However, little is known about normal spatial variations in shear wave speed along the Achilles tendon.

Therefore, the purpose of this study was to investigate spatial variations in shear wave speed along medial and lateral paths of the Achilles tendon for three different ankle postures: resting ankle angle (R, i.e. neutral), plantarflexed (P; R – 15°), and dorsiflexed (D; R+15°). Prior work has shown greater stretch in the aponeurosis relative to the free tendon (Lieber et al., 1991; Maganaris and Paul, 2000), which may be a result of either intrinsic differences in tendon mechanical properties or changes in tendon cross sectional area. Based on this work, we hypothesized that the distal free Achilles tendon would exhibit greater shear wave speeds than its proximal aponeuroses.

2. Methods

2.1. Experimental protocol

Ten healthy young adults (aged: 26.7 ± 4.1 years, 5M/5F) with no history of tendon injury were recruited for this study. Prior to testing, written consent was obtained from each subject as per the Institutional Review Board requirements. The subject was then asked to walk at a comfortable pace for six minutes to precondition the muscle–tendon unit (Hawkins et al., 2009). Next, the subject was asked to lie prone on an examination table, with their foot extended and hanging off of the edge of the table. A standard clear plastic goniometer was used to measure the resting ankle angle (R, 26.3 ± 5.2° plantarflexion).

Ultrasonic B-mode images and shear wave data were collected using an Aixplorer clinical scanner (Supersonic Imagine; Aix-en-Provence, France; software version 5). All data were collected with the subject relaxed, and hence the plantarflexors in the passive state. The musculoskeletal preset was used with persist set to high and spatial smoothing set to 7. All data were collected by the same sonographer, with light transducer pressure applied. The left edge of a 50 mm linear array transducer (L15-4) was placed over the Achilles tendon distal insertion, and shear wave speed data were collected from five 10 mm × 10 mm boxes (the smallest size allowed) within the imaging field of view. The position of the proximal end of the transducer was then marked using a rubber band placed around the leg, and the transducer was moved proximally such that the distal edge of the transducer aligned with the rubber band, and the data collections were repeated. The transducer was moved proximally, i.e. in 50 mm proximal increments, until the collection location was at least 70 mm proximal of the gastrocnemius muscle–tendon junction. A custom 178 × 127 mm^2 ultrasound standoff pad (Aquaflex, Parker Laboratories, Fairfield, NJ) was used at the two most distal transducer positions. Trials were assigned a path along either the medial or lateral heads of the gastrocnemius (Fig. 1) for three postures: resting ankle angle (R), plantarflexed (P; R+15°), and dorsiflexed (D; R – 15°), in a random order.

2.2. Data analysis

Shear wave speed maps and maps of the quality of the shear wave speed estimates were stored in DICOM images exported from the system, and data were extracted using a research package script. A region-of-interest (ROI) was manually defined within the tendon for all images (Fig. 2) using a custom Matlab (Version 7.14) graphical user interface (GUI). The tendon was delineated from the muscle and surrounding tissue by looking for changes in echogenic intensity and echotexture on a given B-mode image in the region where shear wave speed was measured. Subsequently, the shear wave speed data were extracted from this ROI. From the ROI data, several parameters were computed, including the mean shear wave speed, ROI thickness, and ROI depth. ROI thickness was measured by finding the average number of pixels per column in the ROI and multiplying this number by the known distance per pixel (mm/pixel). ROI depth was measured by calculating the location of the center of mass of the ROI and measuring the distance to the skin surface. The spatial location of anatomical landmarks (calcaneus insertion (CI), soleus junction (SJ), and gastrocnemius aponeurosis (AP)) were measured from B-mode images (Fig. 2), with the CI defined as the start of the imaging path (0 mm). Because the locations of these landmarks vary (O'Brien, 1984), data were interpolated between them as follows: from the CI to SJ, the SJ to the AP (divided into three equally sized regions), and the AP+70 mm.

We also investigated the fidelity of the shear wave speed measurements using two metrics. First, we measured the quality of the shear wave speed estimates, which were also extracted from the user-defined ROI within the DICOM images using the research script. The quality metric is derived from the cross-correlation method used to estimate shear wave speed. Shear wave speed is estimated by tracking the shear wave using cross correlation, which compares the similarity of the shear wave shape at one time point to a later time point by convolving the two wave signals. The similarity of the waveforms is described by the correlation coefficient (values ranging from 0 to 1). Thus, a higher correlation coefficient would correspond with higher quality tracking and a higher fidelity shear wave speed estimate. Secondly, we calculated data saturation, which we calculated as the ratio of the pixels in the ROI at the maximum trackable shear wave speed of the system (16.3 m/s) divided by the total pixels.

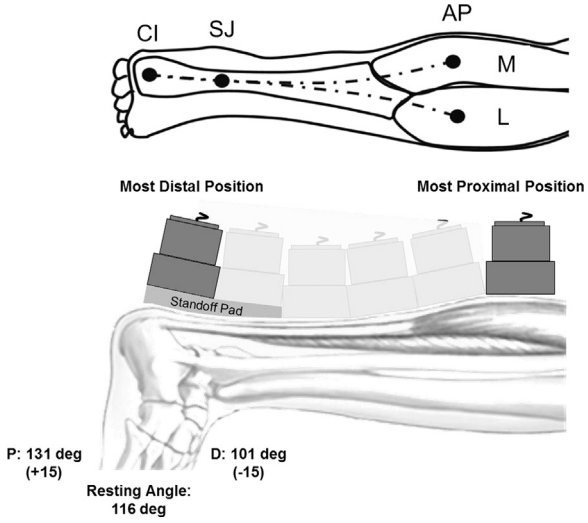

Fig. 1. Experimental methods. Shear wave speed was measured along two paths: medial (M) and lateral (L), for three different postures: plantarflexed (P), resting ankle angle (R), and dorsiflexed (D). Data were collected from an average of six transducer positions from the calcaneus insertion to 70 mm beyond the gastrocnemius muscle–tendon junction. Portions of this figure adapted from *Healthwise, Incorporated*.

Please cite this article as: DeWall, R.J., et al., Spatial variations in Achilles tendon shear wave speed. Journal of Biomechanics (2014), http://dx.doi.org/10.1016/j.jbiomech.2014.05.008

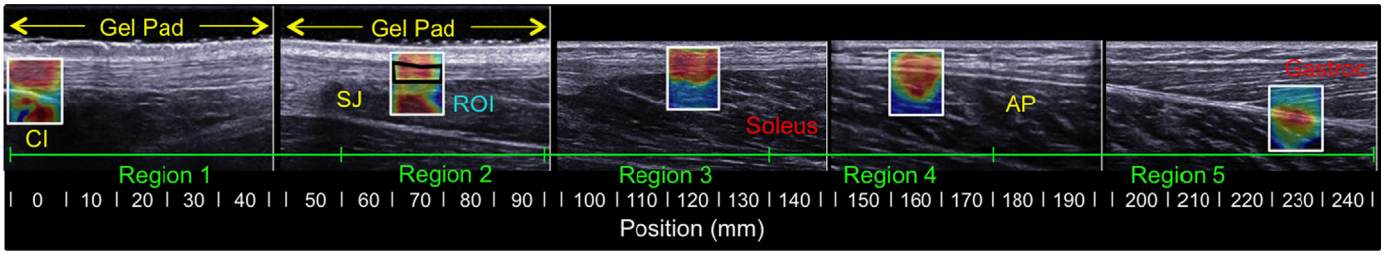

Fig. 2. Representative example of images obtained along a medial path at the resting ankle angle (R). A custom standoff pad was used for the first two transducer positions. Shear wave speed was measured within five boxes per transducer position (only one shown per position for clarity). After collection, an ROI (text shown in cyan, ROI drawn in black for clarity) was defined within the tendon using a custom GUI. Anatomical landmarks, i.e. the calcaneus insertion (CI), soleus junction (SJ), and aponeurosis (AP), were then used to divide the Achilles tendon shear wave speed data into five regions.

2.3. Statistical analysis

The statistical analysis was completed using the R statistics package (http://www.r-project.org). In region 1, the Achilles tendon has yet to diverge into medial and lateral segments. Thus, the transducer was in the same location for both paths, i.e. medial location=lateral location. Because of this, postural (P, R) differences in shear wave speed were assessed using a one-way analysis of variance (ANOVA; $p<0.05$). The dorsiflexed (D) data were removed because of high shear wave speed saturation in this region (> 10%). Post hoc analysis was performed using Tukey multiple comparisons ($^{\dagger}p<0.05$; $^{\ddagger}p<0.001$).

Proximal to region 2, the Achilles tendon diverges into medial and lateral segments. Thus, in regions 3–5, spatial differences in shear wave speed were assessed using a three-way ANOVA with posture (P, R, D), side (medial, lateral), and region (3,4,5) as factors. Region 2 was omitted because this was the location where the medial and lateral paths diverged. Post hoc analysis compared shear wave speed in adjacent regions ($^{*}p<0.05$; $^{**}p<0.001$) and sides within a region (medial vs. lateral; $^{\S}p<0.05$; $^{\S\S}p<0.05$) for the resting ankle angle.

To investigate the potential influence of depth and thickness on shear wave speed, univariate linear regression was used to find the best fit line of shear wave speed to thickness or depth for the plantarflexed and resting ankle angle postures (dorsiflexed posture data were removed because of saturation). The data from the gastrocnemius aponeuroses were excluded from the regression analysis because of the potential influence of the thickening layer of muscle posterior to the tendon, which is not present in the free tendon and soleus aponeurosis.

Finally, the repeatability of measurements was evaluated by calculating the coefficient of variation (CV). For a given image, two different observers independently defined the tendon ROIs where shear wave speeds were measured.

3. Results

Achilles tendon shear wave speed varied significantly with spatial location and ankle angle. The average shear wave speed in the free tendon (region 1) increased from 7.2 to 12.0 m/s between the plantarflexed and neutral positions (Fig. 3, $p<0.0001$). Shear wave speeds in the dorsiflexed position were over 10% saturated in regions 1 and 2 (Table 1). Shear wave speeds were highest in the free tendon and decreased moving proximally toward the gastrocnemius muscle–tendon junctions (Fig. 4). The only exception to this was a slight increase in shear wave speed between the calcaneus insertion and soleus muscle–tendon junction in the plantarflexed posture. Shear wave speeds decreased more rapidly along the lateral path than along the medial path. In regions 3–5, shear wave speeds decreased significantly in the distal–proximal direction (Fig. 5; regions 3 and 4, p=0.0047; regions 4 and 5, $p<0.0001$). Additionally, the shear wave speed was significantly higher along the medial path when compared to the lateral path (region 3, $p=0.00067$; region 4, $p=0.00016$; region 5, $p<0.0001$).

Tendon thickness was greatest between the calcaneus insertion and soleus muscle–tendon junction (5.10 ± 0.55 mm; Fig. 6) and decreased proximally along both paths, reaching 1.39 ± 0.29 mm and 1.58 ± 0.22 mm at the medial and lateral gastrocnemius muscle–tendon junctions, respectively. Tendon depth increased at a fairly constant rate from the calcaneus insertion to the musculotendinous junction, at which point the rate of depth change increased.

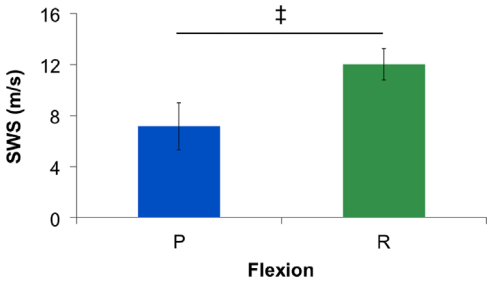

Fig. 3. Shear wave speed in the free tendon varied significantly ($^{\dagger}p<0.05$; $^{\ddagger}p<0.001$) between plantarflexed (P) and resting ankle angle (R) postures. Data from the dorsiflexed (D) posture were omitted because of excessive data saturation (> 10%). Note that because the first transducer position was the same for the medial and lateral paths, all trials from both paths were averaged.

In most cases, shear wave speed decreased with decreasing thickness and increasing depth (Fig. 7), but their correlation with shear wave speed was quite low for both mean ROI thickness (mean $R^2\sim0.34$) and depth (mean $R^2\sim0.43$). The average CV between two observers was 0.156.

4. Discussion

We investigated spatial variations in Achilles tendon shear wave speed from the calcaneus insertion to the medial and lateral gastrocnemius aponeuroses. Our results show that shear wave speed is closely linked to the spatial position along the Achilles tendon, varies between the medial and lateral sides, and depends directly on ankle posture. These observations demonstrate the critical importance of considering both spatial location and posture when using SSI for biomechanical or clinical evaluations of the Achilles tendon.

Our shear wave speed measurements within the free tendon were comparable to prior studies (Table 2) and preliminary data from the aponeurosis (Chernak et al., 2012). In some studies, the Young's modulus (E) or the shear elastic modulus (μ) were reported, which we converted to shear wave speed using the relationships $E=3\rho v^2$ and $\mu=\rho v^2$, where ρ is the tissue density (assumed to be 1000 kg/m^3) and v is the tissue shear wave speed. Although commercial SSI systems can display tissue elasticity in terms of either shear wave speed or the Young's modulus, the Young's modulus computation assumes tissue isotropy, which does not hold for the anisoptropic tendon (Kuo et al., 2001; Royer et al., 2011). For this reason, we chose to report values in terms of shear wave speed.

Achilles tendon shear wave speeds increased substantially with dorsiflexion. This result reflects the strain-stiffening behavior that tendinous tissue exhibits at low loads as slack fibers become taut (Fung, 1993). These observations are consistent with prior measurements taken when passively stretching muscle (Chernak

Table 1
Summary of shear wave speed data saturation by region.

Side	Posture	Saturation (%)				
		Region 1	Region 2	Region 3	Region 4	Region 5
Medial	Plantarflexion	0.2 ± 1.1	0.0 ± 0.0	0.0 ± 0.0	0.0 ± 0.0	0.02 ± 0.2
Medial	Resting ankle angle	5.2 ± 8.5	2.2 ± 4.1	1.2 ± 3.9	0.0 ± 0.0	0.0 ± 0.0
Medial	Dorsiflexion	16.7 ± 16.1	16.1 ± 14.7	6.5 ± 9.1	0.7 ± 2.1	1.1 ± 6.5
Lateral	Plantarflexion	0.2 ± 1.1	0.0 ± 0.0	0.0 ± 0.0	0.0 ± 0.0	0.0 ± 0.0
Lateral	Resting ankle angle	4.8 ± 9.2	1.2 ± 4.2	0.1 ± 0.8	0.0 ± 0.0	0.0 ± 0.0
Lateral	Dorsiflexion	18.9 ± 16.8	10.4 ± 14.0	3.5 ± 8.6	0.3 ± 1.4	0.0 ± 0.0

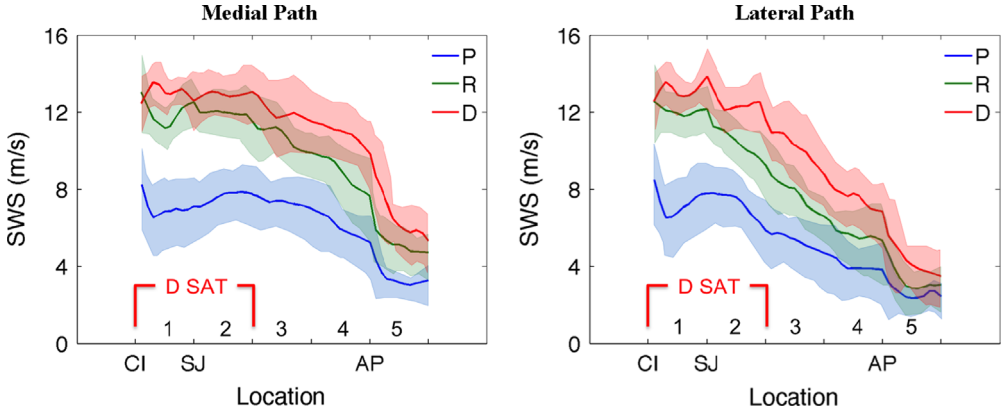

Fig. 4. Average shear wave speeds (+/- one standard deviation) from plantarflexed (P), resting ankle angle (R), and dorsiflexed (D) postures. Both medial and lateral paths exhibit a distal to proximal reduction in shear wave speed, with the transition occurring more distally along the lateral path. Note that data for the dorsiflexed posture in regions 1 and 2 had greater than 10% pixel saturation (D SAT), which results in underestimation of the true shear wave speed.

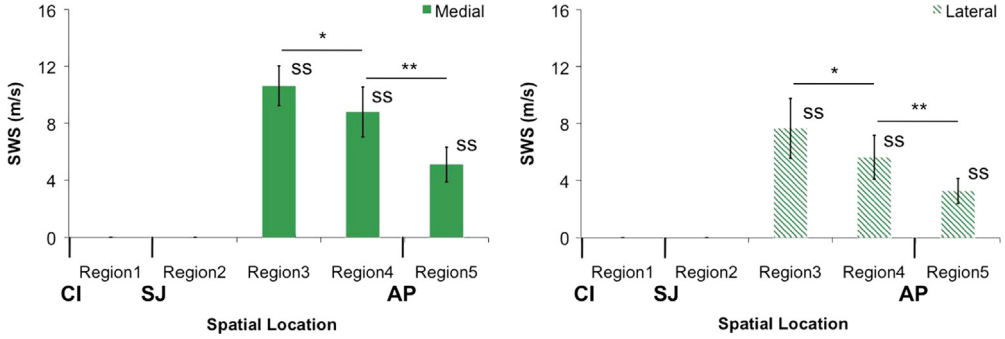

Fig. 5. Spatial variations in shear wave speed in the resting ankle angle posture (R) for medial and lateral paths for regions 3–5. Data from regions 1 and 2 were omitted because the transducer paths had not sufficiently diverged to consider the sides distinct (see Fig. 1). Shear wave speed decreased significantly moving from the calcaneus insertion to the gastrocnemius aponeurosis ($^{*}p < 0.05$; $^{**}p < 0.001$). Note that only adjacent regions were compared for clarity. Medial and lateral paths were also compared in each region. Shear wave speed was significantly higher along the medial path ($^{s}p < 0.05$; $^{ss}p < 0.001$) in the soleus and gastrocnemius aponeuroses.

et al., 2013) and tendon (Aubry et al., 2013; Hug et al., 2013). It is possible that tendon relaxation could influence the shear wave speed measurements in the dorsiflexed posture. However, in a pilot study, we measured tendon and aponeurosis shear wave speeds in a dorsiflexed posture (−15°) every minute for 30 consecutive minutes. We observed no significant temporal changes in shear wave speed over the 30 min interval. Postural effects were most pronounced in the free Achilles tendon, with the shear wave speed increasing an average of 67% when moving from a plantarflexed to resting ankle angle position. The dorsiflexed posture could not be compared to the plantarflexed and resting ankle postures because saturation (> 10% of data; Table 1, Fig. 8) led to an underestimation of the shear wave speed. Achilles tendinopathies and tears often occur in the free tendon (Jozsa et al., 1989). B-mode ultrasound imaging is used clinically to assess Achilles tendon damage but cannot provide a quantitative assessment of tendon mechanical integrity. The emergence of SSI provides a potential quantitative tool for evaluating tendon mechanical properties in normal and damaged states (Arda et al., 2011; Aubry et al., 2013; Chen et al., 2013; DeWall et al., 2014; Hug et al., 2013), given the dependence of shear wave speed on tissue elasticity (Bercoff et al., 2004; Royer et al., 2011). Our observations indicate the importance of standardizing SSI clinical examination techniques, as subtle variations in limb posture can substantially alter the measured shear wave speed.

There has long been interest among biomechanists about the relative stiffness of tendinous and aponeurosis tissue, but it remains challenging to assess aponeurosis properties within a musculotendon unit. An early study by Lieber et al. (1991) on the frog semintendinosis tendon showed significantly higher strains in the aponeurosis (8%) than the tendon (2%) during passive stretch, suggesting the aponeurosis is more compliant. Subsequent human *in vivo* studies on the Achilles tendon have reported conflicting results, with some studies showing higher strains in the aponeurosis than the tendon (Maganaris and Paul, 2000), no differences in strain (Muramatsu et al., 2001), or higher strains in the

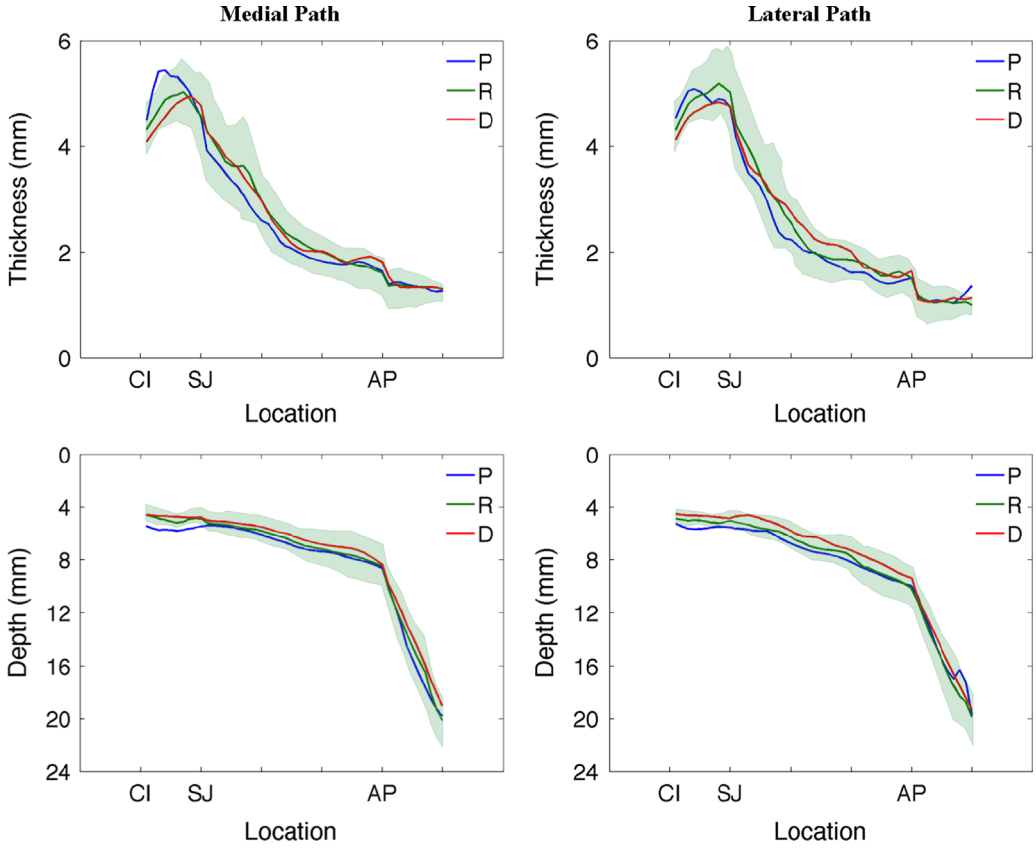

Fig. 6. Tendon thickness and depth varied along the length of the Achilles tendon for plantarflexed (P), resting ankle angle (R), and dorisflexed (D) postures. The thickness decreases proximally, with the thickest region of the tendon occurring in the free tendon between the calcaneus insertion (CI) and the soleus junction (SJ). Depth increases after the CI, with a distinct change in the rate of depth increase beyond the gastrocnemius muscle–tendon junction (AP).

tendon (Magnusson et al., 2003). Our data clearly show a gradual reduction in shear wave speed from the free tendon to the gastrocnemius aponeurosis, supporting the idea that the aponeurosis provides a more compliant interface between the free tendon and muscle tissue. This result has potential implications for musculoskeletal models that typically assume uniform mechanical properties for the tendon and aponeurosis (Arnold et al., 2010; Blemker and Delp, 2005).

We also found significant differences in shear wave speed in the medial and lateral aspects of the Achilles tendon, with the medial aspects of the proximal tendon exhibiting higher speeds than the lateral side (Fig. 5). Such variations in shear wave speed could arise from greater innate tissue stiffness or higher passive tension on the medial side. Anatomically, the medial gastrocnemius muscle is longer than the lateral gastrocnemius (Antonios and Adds, 2008; Ward et al., 2009; Wickiewicz et al., 1983). This difference was notable in our study, with the medial gastrocnemius musculotendon junction extending an average of 31 mm more distally than the lateral musculotendon junction. Thus, it is possible that the differences in shear wave speed reflect differences in the medial and lateral transition region between the free tendon and its insertion onto the gastrocnemius muscle fibers. Other potential factors include medio-lateral variations in the patterns in which the tendon fibers originate from the muscle–tendon junction (Szaro et al., 2009) and the inversion angle of the foot. We did not actively control or measure the inversion angle, but we did try to maintain a subject's unloaded, neutral inversion angle for both the dorsiflexion and plantarflexion trials.

We measured tendon thickness and depth to evaluate if the changing size and spatial position of the tendon was related to variations in shear wave speed. Univariate linear regression showed significant, albeit weak correlation, between shear wave speed, thickness, and depth measures (Fig. 7). Aubry et al. (2013) likewise found that the tendon thickness did not predict shear wave speed variations over a cross-section of subjects. Numerically, our thickness measurements near the calcaneus insertion are consistent with Aubry et al. (2013) (4.4 ± 0.6 mm). Tendon thickness decreased when moving the transducer proximally. Although our analysis does not strongly correlate thickness with shear wave speed, it has recently been shown that the Achilles tendon's aligned structure and boundaries influence shear wave propagation (Brum et al., 2014). Further basic studies are needed to fully elucidate the effect of boundary conditions and fiber alignment on shear wave propagation. Shear wave speed decreased with increasing depth. This result is relevant because acoustic waves exhibit depth-dependent attenuation, with high frequency components preferentially attenuated (Bamber, 1986). Thus, in a given material, shear waves generated deeper in tissue will be composed of lower frequency components. Because soft tissues are dispersive materials (Brum et al., 2014; Deffieux et al., 2009), i.e. exhibit frequency-dependence, the shear wave speed may decrease with increasing depth. However, it should be noted that in our study, changes in depth and transducer spatial location were confounding factors. Thus, changes in shear wave speed with depth may just reflect changes in tendon material properties as the transducer was moved proximally toward the aponeurosis.

We also investigated shear wave speed measurement fidelity by measuring the quality of the shear wave speed estimates. The shear wave speed estimate quality provides a measure of the similarity of the shear wave at the site of generation with the wave at a later time point, i.e. after it propagates through the tendon. Lower quality indicates poorer tracking, and thus a lower fidelity

Please cite this article as: DeWall, R.J., et al., Spatial variations in Achilles tendon shear wave speed. Journal of Biomechanics (2014), http://dx.doi.org/10.1016/j.jbiomech.2014.05.008

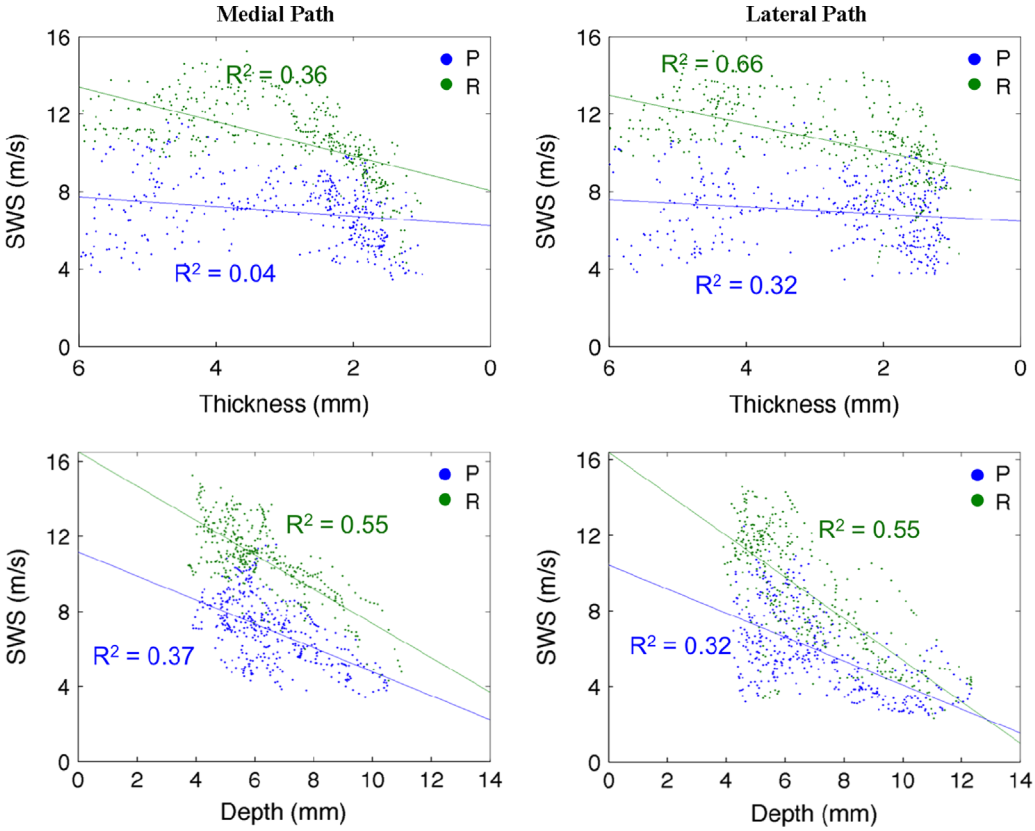

Fig. 7. Univariate regression analysis showing the relationship between shear wave speed and depth or thickness along each path (medial or lateral) for plantarflexed (P) and resting ankle angle (R) postures. The dorisflexed (D) posture was omitted because of excessive (> 10%) saturation in regions 1 and 2. Least-squares fits were significant ($p < 0.001$) but exhibited relatively weak correlations.

Table 2
Compilation of tendon shear wave speeds from prior studies.

Reference	Description	Ankle angle	*n*	Shear wave speed (m/s)			
				Mean		Std	
Aubry et al., 2011	Healthy Achilles	Maximum plantarflexion	30	5.8	±	3.9	*
Aubry et al., 2013	Healthy Achilles	Maximum plantarflexion	80	6.8	±	1.4	
Aubry et al., 2013	Healthy Achilles	Plantarflexion (135°)	80	10.7	±	2.4	
Arda et al., 2011	Healthy Achilles	Resting ankle angle	127	4.1	±	2.9	*
Chen et al., 2010	Asymptomatic Achilles	Resting ankle angle	36	9.9	±	1.2	*
Chen et al., 2010	Ruptured Achilles	Resting ankle angle	14	4.3	±	4.8	*
Hug et al., 2013	Healthy Achilles	Plantarflexion (140°)	9	5.9	±	2.6	+
Kot et al., 2012	Healthy patellar tendon	Resting angle	20	4.8	±	3.3	*

*Indicates that the shear wave speed (ν) is converted from a reported elastic modulus. Shear wave speed is computed by assuming: $E=3\rho\nu^2$, with $\rho=1000$ kg/m^3 (Aubry et al., 2013).
+Indicates that shear wave speed is converted from a reported shear elastic modulus. Shear wave speed is computed by assuming $\mu=\rho\nu^2$ (Hug et al., 2013).

shear wave speed estimate. We found that quality was the lowest at the calcaneus insertion, which is likely due to the presence of bone. The intense acoustic backscatter off of the reflective bone interface can induce acoustic wave mode conversion (e.g. a compressional wave to a shear wave) that may interfere with shear wave tracking. Quality was high and relatively constant throughout the rest of the tendon for all postures (~0.92), suggesting that the induced shear waves propagated with relatively little dispersion over the analysis regions used in this study.

Tendon tissue is quite stiff relative to other soft tissues, which results in higher shear wave speeds and the potential for saturation to occur when the speed exceeds the tracking capacity of current shear wave imaging systems. To evaluate this, we computed the percent of saturated pixels (16.3 m/s) within our ROIs. We found almost no saturation in the plantarflexed posture, slight saturation (~5%) in the neutral position in the free tendon and soleus aponeurosis, and high saturation (over 10% in regions 1 and 2) in the dorsiflexed posture (Table 1, Fig. 8). This latter result likely explains why we observed a smaller increase in shear wave speed between the neutral and dorsiflexed positions than between the plantarflexed and neutral positions in regions 1 and 2 (Fig. 4). Because of this, the dorsiflexed data in these regions were removed from our statistical analysis. Data from prior SSI studies suggest that saturation may be an issue. For example, Aubry, et al. (2013) reported shear wave speeds of 15.5 ± 0.9 m/s and 16.1 ± 0.7 m/s in neutral and dorsiflexed postures, respectively. An *ex vivo* tendon study reported decreasing repeatability with increasing tendon load (Peltz et al., 2013), which could arise in part from underlying saturation effects. It should be noted that we only measured SWS at $\pm 15°$ from the resting ankle angle (116°).

Please cite this article as: DeWall, R.J., et al., Spatial variations in Achilles tendon shear wave speed. Journal of Biomechanics (2014), http://dx.doi.org/10.1016/j.jbiomech.2014.05.008

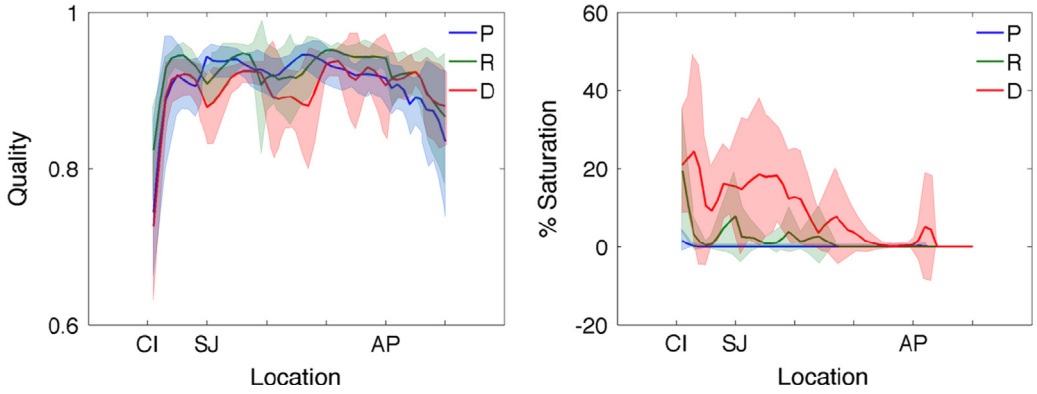

Fig. 8. Quality and percent saturation from the calcaneus insertion (CI) to the medial gastrocnemius aponeurosis (AP) for plantarflexed (P), resting ankle angle (R), and dorisflexed (D) postures. The quality of the shear wave speed estimates was relatively constant, with the exception of measurements taken near the CI. There was little measurement saturation in the plantarflexed posture. However, in the dorsiflexed posture, over 10% of pixels registered the maximum measurable shear wave speed of 16.3 m/s in regions 1 and 2. Note that shear wave speed estimate quality and percent saturation were similar along the lateral path.

Thus, the ankle angle was still 111° in the dorsiflexed (D) posture, which is still considerably below the dorsiflexion range of motion of a healthy individual (8–26° beyond 90°, Rome, 1996). From these observations, we conclude that modest stretching of the healthy Achilles tendon can result in measurement saturation (shear wave speeds > 16.3 m/s), leading to underestimation of the actual shear wave speed. This emphasizes the importance of performing shear wave imaging of the Achilles tendon in resting or plantarflexed positions. It should be noted that this conclusion applies only to the current software version of the system (version 5). Future versions of this system or new devices may increase the maximum shear wave speed that can be measured. Additionally, spatial smoothing may influence the measured shear wave speed, particularly if there is a large differential in tissue stiffness in the vicinity of the shear wave speed ROI. Care must be taken to use the same smoothing setting throughout the course of a study. In cases of tendon pathology, saturation may be less problematic. That is, an increase in tendon compliance with tendinopathy (De Zordo et al., 2010) may lower shear wave speeds to within the measurable range of the system.

There are a few limitations to this study. A prior study has shown that transducer pressure can significantly affect shear wave speed measurements in muscle and tendon (Kot et al., 2012). Although we were careful to apply light pressure during data collections, it is possible that transducer pressure varied. Although we evaluated the reliability of ROI delineations, it has been shown that the absolute repeatability of SSI measures can vary across sonographers (Aubry et al., 2013; Lacourpaille et al., 2012; Peltz et al., 2013). It would therefore be interesting to evaluate the consistency of our results on datasets collected by different sonographers. Prior studies have investigated the potential relationship between tendon shear wave speed and a variety of factors, including gender (Arda et al., 2011; Aubry et al., 2013), activity level (Aubry et al., 2011, 2013), and age (Arda et al., 2011; Aubry et al., 2013). Of these parameters, we only investigated a potential relationship between shear wave speed and gender. We did not find a correlation, though it should be noted that we had little statistical power with our small subject population (5F/5M).

In summary, we showed spatial-dependent changes in shear wave speed in the Achilles free tendon, soleus aponeurosis, and aponeuroses of the medial and lateral gastrocnemius. Taken together, these observations suggest that transducer positioning and ankle posture must be monitored to appropriately interpret shear wave speed measurements. Additionally, it may be necessary to evaluate the tendon in the resting or a plantarflexed position to avoid measurement saturation. With further investigation, tendon shear wave imaging holds promise as a complementary quantitative evaluation tool to traditional clinical morphological assessment.

Conflict of interest statement

The authors declare that they have no conflicts of interest with regards to this work.

Acknowledgments

The authors would like to acknowledge the support of the University of Wisconsin Radiology Research and Development Fund (Grant No. 1204-001) and NIH F31AG043216. We would also like to thank Alex Ehlers for assistance with the data analysis.

References

Antonios, T., Adds, P.J., 2008. The medial and lateral bellies of gastrocnemius: a cadaveric and ultrasound investigation. Clin. Anat. 21, 66–74.
Arampatzis, A., Stafilidis, S., DeMonte, G., Karamanidis, K., Morey-Klapsing, G., Bruggenmann, G.P., 2005. Strain and elongation of the human gastrocnemius tendon and aponeurosis during maximal plantarflexion effort. J. Biomech. 38, 833–841.
Arda, K., Ciledag, N., Aktas, E., Aribas, B.K., Kose, K., 2011. Quantitative assessment of normal soft-tissue elasticity using shear-wave ultrasound elastography. Am. J. Roentgenol. 197, 532–536.
Arndt, A.N., Komi, P.V., Bruggemann, G.P., Lukkariniemi, J., 1998. Individual muscle contributions to the in vivo achilles tendon force. Clin. Biomech. 13, 532–541.
Arnold, E.M., Ward, S.R., Lieber, R.L., Delp, S.L., 2010. A model of the lower limb for analysis of human movement. Ann. Biomed. Eng. 38, 269–279.
Athanasiou, A., Tardivon, A., Tanter, M., Sigal-Zafrani, B., Bercoff, J., Deffieux, T., Gennisson, J.L., Fink, M., Neuenschwander, S., 2010. Breast lesions: quantitative elastography with supersonic shear imaging–preliminary results. Radiology 256, 297–303.
Aubry, S., Risson, J.R., Barbier-Brion, B., Tatu, L., Vidal, C., Kastler, B., 2011. Transient elastography of calcaneal tendon: preliminary results and future prospects. J. Radiol. 92, 421–427.
Aubry, S., Risson, J.R., Kastler, A., Barbier-Brion, B., Siliman, G., Runge, M., Kastler, B., 2013. Biomechanical properties of the calcaneal tendon in vivo assessed by transient shear wave elastography. Skelet. Radiol. 42, 1143–1150.
Bamber, J.C., 1986. Attenuation and absorption. In: Hill, C. (Ed.), Physical Properties of Medical Ultrasonics. Halsted Press, New York, pp. 118–199.
Bavu, E., Gennisson, J.L., Couade, M., Bercoff, J., Mallet, V., Fink, M., Badel, A., Vallet-Pichard, A., Nalpas, B., Tanter, M., Pol, S., 2011. Noninvasive in vivo liver fibrosis evaluation using supersonic shear imaging: a clinical study on 113 hepatitis C virus patients. Ultrasound Med. Biol. 37, 1361–1373.
Bercoff, J., Tanter, M., Fink, M., 2004. Supersonic shear imaging: a new technique for soft tissue elasticity mapping. IEEE Trans. Ultrason. Ferroelectr. Freq. Control 51, 396–409.
Blemker, S.S., Delp, S.L., 2005. Three-dimesional represenation of complex muscle architectures and geometries. Ann. Biomed. Eng. 33, 661–673.
Bouillard, K., Nordez, A., Hug, F., 2011. Estimation of individual muscle force using elastography. PLoS One 6, e29261.

Brum, J., Bernal, M., Gennisson, J.L., Tanter, M., 2014. in vivo evaluation of the elastic anisotropy of the human Achilles tendon using shear wave dispersion analysis. Phys. Med. Biol. 59, 505–523.
Chen, X.M., Cui, L.G., He, P., Shen, W.W., Qian, Y.J., Wang, J.R., 2013. Shear wave elastographic characterization of normal and torn achilles tendons: a pilot study. J. Ultrasound Med. 32, 449–455.
Chernak, L.A., DeWall, R.J., Lee, K.S., Thelen, D.G., 2013. Length and activation dependent variations in muscle shear wave speed. Physiol. Meas. 34, 713–721.
Chernak, L.A., DeWall, R.J., Thelen, D., 2012. Posture and activation dependent variations in shear wave speed in the gastrocnemius muscle and aponeurosis. In American Society of Biomechanics, Gainesville, FL.
D'Onofrio, M., Gallotti, A., Mucelli, R.P., 2010. Tissue quantification with acoustic radiation force impulse imaging: measurement repeatability and normal values in the healthy liver. Am. J. Roentgenol. 195, 132–136.
De Zordo, T., Chhem, R., Smekal, V., Feuchtner, G., Reindl, M., Fink, C., Faschingbauer, R., Jaschke, W., Klauser, A.S., 2010. Real-time sonoelastography: findings in patients with symptomatic achilles tendons and comparison to healthy volunteers. Ultraschall in der Med. 31, 394–400.
De Zordo, T., Lill, S.R., Fink, C., Feuchtner, G.M., Jaschke, W., Bellmann-Weiler, R., Klauser, A.S., 2009. Real-time sonoelastography of lateral epicondylitis: comparison of findings between patients and healthy volunteers. Am. J. Roentgenol. 193, 180–185.
Deffieux, T., Montaldo, G., Tanter, M., Fink, M., 2009. Shear wave spectroscopy for in vivo quantification of human soft tissues visco-elasticity. IEEE Trans. Med. Imaging 28, 313–322.
DeWall, R.J., Jiang, J., Wilson, J., Lee, K.S., 2014. Visualizing tendon elasticity in an ex vivo partial tear model. Ultrasound Med. Biol. 40, 158–167.
Fahlstrom, M., Jonsson, P., Lorentzon, R., Alfredson, H., 2003. Chronic Achilles tendon pain treated with eccentric calf-muscle training. Knee Surg. Sports Traumatol. Arthrosc. 11, 327–333.
Finni, T., Hodgson, J.A., Lai, A.M., Edgerton, V.R., Sinha, S., 2003. Nonuniform strain of human soleus aponeurosis-tendon complex during submaximal voluntary contractions in vivo. J. Appl. Physiol. 95, 829–837.
Fung, Y.C., 1993. Biomechanics: Mechanical Properties of Living Tissues. Springer, New York, pp. 242–320.
Gennisson, J.L., Deffieux, T., Mace, E., Montaldo, G., Fink, M., Tanter, M., 2010. Viscoelastic and anisotropic mechanical properties of in vivo muscle tissue assessed by supersonic shear imaging. Ultrasound Med. Biol. 36, 789–801.
Hawkins, D., Lum, C., Gaydos, D., Dunning, R., 2009. Dynamic creep and preconditioning of the Achilles tendon in-vivo. J. Biomech. 42, 2813–2817.
Hug, F., Lacourpaille, L., Maisetti, O., Nordez, A., 2013. Slack length of gastrocnemius medialis and Achilles tendon occurs at different ankle angles. J. Biomech. 46, 2534–2538.
Jozsa, L., Kvist, M., Balint, B.J., Reffy, A., Jarvinen, M., Lehto, M., Barzo, M., 1989. The role of recreational sport activity in Achilles tendon rupture. A clinical, pathoanatomical, and sociological study of 292 cases. Am. J. Sports Med. 17, 338–343.
Koo, T.K., Guo, J.Y., Cohen, J.H., Parker, K.J., 2013. Relationship between shear elastic modulus and passive muscle force: an ex-vivo study. J. Biomech. 46, 2053–2059.
Kot, B.C., Zhang, Z.J., Lee, A.W., Leung, V.Y., Fu, S.N., 2012. Elastic modulus of muscle and tendon with shear wave ultrasound elastography: variations with different technical settings. PLoS One 7, e44348.
Kubo, K., Kawakami, Y., Fukunaga, T., 1999. Influence of elastic properties of tendon structures on jump performance in humans. J. Appl. Physiol. 87, 2090–2096.
Kuo, P.-L., Li, P.-C., Li, M.-L., 2001. Elastic properties of tendon measured by two different approaches. Ultrasound Med. Biol. 27, 1275–1284.
Lacourpaille, L., Hug, F., Bouillard, K., Hogrel, J.Y., Nordez, A., 2012. Supersonic shear imaging provides a reliable measurement of resting muscle shear elastic modulus. Physiol. Meas. 33, N19–N28.
Lieber, R.L., Leonard, M.E., Brown, C.G., Trestik, C.L., 1991. Frog semitendinosis tendon load–strain and stress–strain properties during passive loading. Am. J. Physiol. 261, C86–C92.
Maganaris, C.N., 2003. Tendon conditioning: artefact or property? Proc. R. Soc. – Biol. Sci. 270 (Supplement 1), S39–S42.
Maganaris, C.N., Paul, J.P., 1999. in vivo human tendon mechanical properties. J. Physiol. 521 (Pt 1), 307–313.
Maganaris, C.N., Paul, J.P., 2000. Load-elongation characteristics of in vivo human tendon and aponeurosis. J. Exp. Biol. 203, 751–756.
Maganaris, C.N., Paul, J.P., 2002. Tensile properties of the in vivo human gastrocnemius tendon. J. Biomech. 35, 1639–1646.
Magnusson, S.P., Aagaard, P., Dyhre-Poulsen, P., Kjaer, M., 2001. Load–displacement properties of the human triceps surae aponeurosis in vivo. J. Physiol. 531, 277–288.
Magnusson, S.P., Hansen, P., Aagaard, P., Brond, J., Dyhre-Poulsen, P., Bojsen-Moller, J., Kjaer, M., 2003. Differential strain patterns of the human gastrocnemius aponeurosis and free tendon, in vivo. Acta Physiol. Scand. 177, 185–195.
Maisetti, O., Hug, F., Bouillard, K., Nordez, A., 2012. Characterization of passive elastic properties of the human medial gastrocnemius muscle belly using supersonic shear imaging. J. Biomech. 5, 978–984.
Muramatsu, T., Muraoka, T., Takeshita, D., Kawakami, Y., Hirano, Y., Fukunaga, T., 2001. Mechanical properties of tendon and aponeurosis of human gastrocnemius muscle in vivo. J. Appl. Physiol. 90, 1671–1678.
Nightingale, K., Soo, M.S., Nightingale, R., Trahey, G., 2002. Acoustic radiation force impulse imaging: in vivo demonstration of clinical feasibility. Ultrasound Med. Biol. 28, 227–235.
Nordez, A., Hug, F., 2010. Muscle shear elastic modulus measured using supersonic shear imaging is highly related to muscle activity level. J. Appl. Physiol. 108, 1389–1394.
O'Brien, T., 1984. The needle test for complete rupture of the Achilles tendon. J. Bone Jt. Surv. 66, 1099–1101.
Ophir, J., Céspedes, I., Ponnekanti, H., Yazdi, Y., Li, X., 1991. Elastography: a quantitative method for imaging the elasticity of biological tissues. Ultrason. Imaging 13, 111–134.
Peixinho, C.C., Alves, D.S., Lacerda, R.G., Vieira, T.M.M., Oliveira, L.F., 2008. Strain and slackness of achilles tendon during passive joint mobilization via imaging ultrasonography. Braz. J. Phys. Ther. 12, 366–372.
Peltz, C.D., Haladik, J.A., Divine, G., Siegal, D., van Holsbeeck, M., Bey, M.J., 2013. ShearWave elastography: repeatability for measurement of tendon stiffness. Skelet. Radiol. 42, 1151–1156.
Rome, K., 1996. Ankle joint dorsiflexion measurement studies. A review of the literature. J. Am. Podiatr. Med. Assoc. 86, 205–211.
Royer, D., Gennisson, J.L., Deffieux, T., Tanter, M., 2011. On the elasticity of transverse isotropic soft tissues. J. Acoust. Soc. Am. 129, 2757–2760.
Sandrin, L., Fourquet, B., Hasquenoph, J.M., Yon, S., Fournier, C., Mal, F., Christidis, C., Ziol, M., Poulet, B., Kazemi, F., Beaugrand, M., Palau, R., 2003. Transient elastography: a new noninvasive method for assessment of hepatic fibrosis. Ultrasound Med. Biol. 29, 1705–1713.
Sebag, F., Vaillant-Lombard, J., Berbis, J., Griset, V., Henry, J.F., Petit, P., Oliver, C., 2010. Shear wave elastography: a new ultrasound imaging mode for the differential diagnosis of benign and malignant thyroid nodules. J. Clin. Endocrinol. Metab. 95, 5281–5288.
Szaro, P., Witkowski, G., Smigielski, R., Krajewski, P., Ciszek, B., 2009. Fascicles of the adult human Achilles tendon – an anatomical study. Ann. Anat. 191, 586–593.
Ward, S.R., Eng, C.M., Smallwood, L.H., Lieber, R.L., 2009. Are current measurements of lower extremity muscle architecture accurate? Clin. Orthop. Relat. Res. 467, 1074–1082.
Wickiewicz, T.L., Roy, R.R., Powell, P.L., Edgerton, V.R., 1983. Muscle architecture of the human lower limb. Clin. Orthop. Relat. Res., 275–283.

Please cite this article as: DeWall, R.J., et al., Spatial variations in Achilles tendon shear wave speed. Journal of Biomechanics (2014), http://dx.doi.org/10.1016/j.jbiomech.2014.05.008